Robotica (2016) volume 34, pp. 2140–2150. © Cambridge University Press 2015
doi:10.1017/S0263574715000065

Modeling and friction estimation for wheeled omnidirectional mobile robots

Andre G. S. Conceicao,* Mariane D. Correia and Luciana Martinez

LaR- Robotics Lab and Department of Electrical Engineering, Federal University of Bahia, Rua Aristides Novis, 02, 40210-630, Salvador, BA, Brazil
E-mails: andre.gustavo@ufba.br, marianedc@ufba.br, lucianam@ufba.br

(Accepted January 13, 2015. First published online: February 12, 2015)

SUMMARY
In this study, a model for wheeled mobile robots that includes a static friction model in the force balance at the robot's center of mass is presented. Additionally, a least-squares method to linearly combine functions is proposed to estimate the friction coefficients. The experimental and simulation results are discussed to demonstrate the effectiveness of this approach in indoor environments for two floor types.

KEYWORDS: Mechatronic systems; Mobile robots; Robot Dynamics; Friction; Parameter estimation.

1. Introduction

Modeling of robotic systems is useful for sensitivity analysis,[1,2] prediction,[3,4] and design of controllers.[5,6] When analyzing wheeled mobile robots, where friction effects are critical, it is essential to choose a proper model and controller. The nature of the friction models can be static or dynamic, and the estimation of the parameters can be performed in advance or in real-time. One advantage of using a model that incorporates static friction is that the control technique does not require additional sensors for the detection and compensation of the friction in real-time. The disadvantage is that the parameters in the robot's environment must be identified in advance, as presented in refs. [7] and [8]. In these studies, the parameters were estimated using force sensors in various directions with a repeated set of speeds. Several works have also addressed the problem of friction estimation in the following cases: helical drive in-pipe robot,[9] dynamic model including external wheel forces,[10] and wheel-soil interaction model based on the theory of terramechanics and knowledge of vehicle dynamics.[2]

In this paper, a model that includes a static friction model for omnidirectional wheeled mobile robots is proposed, as well as a new method to parametrically estimate the viscous and Coulomb friction coefficients, and the Stiction force. The method relies on a static friction model and uses a least-squares technique to a linearly combine functions, making possible on-line or in advance parameter estimation. This method uses sensory information about the force and velocity of the robot's center of mass that are likely to be part of wheeled systems. Additionally, the method is computationally efficient and thus suitable for implementation on embedded systems with limited computational resources. Despite of the method of estimation, the main novelty of the proposed model with respect to our previously published approach in[8] is the inclusion of two key friction phenomena in wheeled mobile robots (Stiction force and the Stribeck effect). Simulation and real robot results show the performance of the model for two types of floor. Besides, a comparison with the proposed and previous model shows the large influence of friction on wheeled robots.

* Corresponding author. E-mail: andre.gustavo@ufba.br

https://doi.org/10.1017/S0263574715000065 Published online by Cambridge University Press



(a) (b)

Fig. 1. Wheeled mobile robot and two floor types. (a) Robot. (b) Carpet and synthetic grass.

This article is organized in the following sequence. In Section 2, the wheeled mobile robot and the proposed model are presented. In Section 3, the development of the estimation method is shown. In Section 4, the experimental and simulation results are presented and discussed. Finally, the conclusions are presented in Section 5.

2. Wheeled Mobile Robot

The wheeled mobile robot in Fig. 1(a) is composed of two main modules: a microprocessor system responsible for implementing the system's instrumentation and a time base generation module (sample time of 50 ms) that creates a real time clock. The high-level controllers and the supervisory system are implemented on a personal computer, and these modules communicate through a Zigbee platform. The DC motors are type A-max 22 (nominal voltage: 6 volts, power rating: 5 W) developed by Maxon Motors.[11] These motors have a gear speed reducer with ratio 19:1, and they are controlled by H-bridge circuits. The motors current measurement are done by a shunt resistor in series with the bus of the H-bridge circuits. In addition, each motor is connected to encoders that provides the measurement of the rotational speed. These measurements (current and rotational speed) are used to estimate forces and velocities at the robot's center of mass, respectively. In this paper, two different types of floors were used to analyze the influence of friction on wheeled robots in detail (see Fig. 1(b)).

Because of the vast variations in friction models, it is important to select the proper model structure for a particular system, which is a wheeled omnidirectional mobile robot in this case. Figure 2 shows the voltage ramp response of the robot on synthetic grass and carpet. The friction is larger in cases where the robot only has linear velocities. This result is easily explained by the geometry of the robot. For example, only two of the three motors are active to generate velocities in the v direction. Additionally, the wheels have an angle of 30° to the velocity vector v (see Fig. 3). Figures 2(a) and (b) show the linear velocities (v and v_n), the respective forces (F_v and F_{v_n}) and the applied voltages. In both cases, the Stiction force and the Stribeck effect can be easily detected in the force curves. The Stribeck effect is smaller in angular velocities, where the three motors are active simultaneously in the same direction and with the same input voltages, as shown in Fig. 2(c).

Figure 2(d) shows an example of slippage as a disturbance. In preliminary testing of our three-wheeled robot, slipping occurred only for relative high amplitude voltage step response (>4 V). We can see clearly the moment of slip between the wheels and the field, samples 14–16. As soon as the wheels start to slip, the force drops down to almost zero. The phenomenon shown in Fig. 2(d) was null for voltage ramp responses, as shown in Figs. 2(a) and (b). It is important to say that voltage ramp response and voltage step response with an initial acceleration ramp were used in this paper, so slippage (as a disturbance) between the wheel and the surface motion was avoid in the experiments. Another way to consider the slippage is generally through a percentage of the difference between the surface speed of the wheels. In early odometry calibration (made by a top-view vision system) of our mobile robot, the percentage of slip was estimated for the both motion surface, separately. So, the

https://doi.org/10.1017/S0263574715000065 Published online by Cambridge University Press

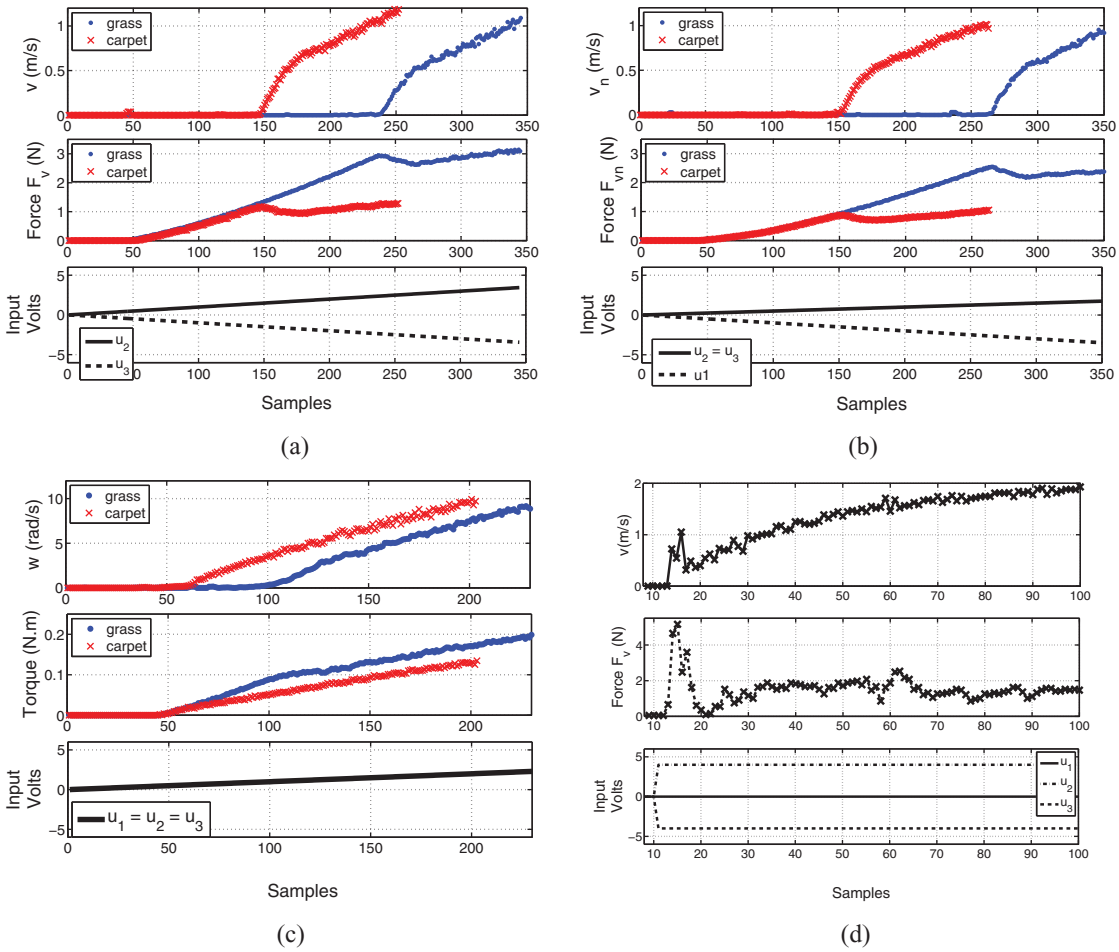


Fig. 2. (a), (b) and (c) Voltage ramp response – grass and carpet. (d) Voltage step response - carpet. u_i are the armature voltages (with $i = 1, 2, 3$).

percentage of slip are considered in the velocities (linear and angular) at the robot's center of mass in an implicitly way.

2.1. Kinematic model

Using the robot coordinate system geometry shown in Fig. 3, the robot kinematic equations of motion can be written as:[12]

$$\begin{bmatrix} \frac{dx_w(t)}{dt} \\ \frac{dy_w(t)}{dt} \\ \frac{d\theta(t)}{dt} \end{bmatrix} = R_o^T(\theta(t)) \begin{bmatrix} v(t) \\ v_n(t) \\ w(t) \end{bmatrix}, \tag{1}$$

where the orthogonal rotation matrix $R_o(\theta(t))$ converts from the global coordinate system to the robot coordinate system and vice-versa.

$$R_o(\theta(t)) = \begin{bmatrix} \cos(\theta(t)) & \sin(\theta(t)) & 0 \\ -\sin(\theta(t)) & \cos(\theta(t)) & 0 \\ 0 & 0 & 1 \end{bmatrix}. \tag{2}$$

The robot pose is represented by the vector $[x_w(t) \;\; y_w(t) \;\; \theta(t)]^T$ that describes the location of the robot in the global coordinate system and the angular difference between the coordinate systems.

https://doi.org/10.1017/S0263574715000065 Published online by Cambridge University Press

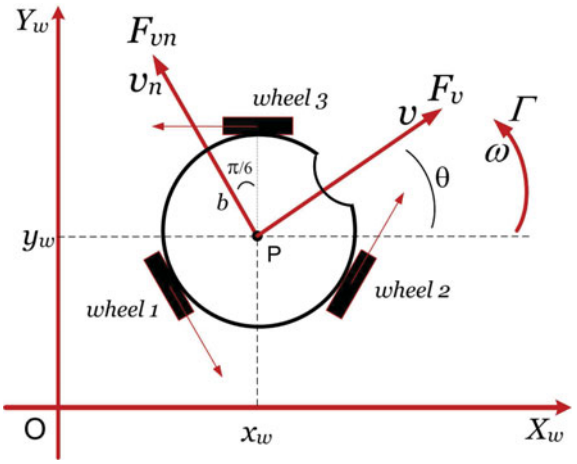


Fig. 3. Coordinate systems and geometric parameters.

The orthogonal components $v(t)$ and $v_n(t)$ of the linear velocity, and the angular velocity $w(t)$ of the robot are represented by the vector $[v(t)\ \ v_n(t)\ \ w(t)]^T$.

The relationship between the robot wheels' angular velocities ($w_{m_i}(t)$, where $i = 1, 2, 3$) and the robot velocities ($v(t)$, $v_n(t)$, $w(t)$) are given by:

$$\begin{bmatrix} v(t) \\ v_n(t) \\ w(t) \end{bmatrix} = (B^T)^{-1} \frac{r}{l} \begin{bmatrix} w_{m_1}(t) \\ w_{m_2}(t) \\ w_{m_3}(t) \end{bmatrix}, \tag{3}$$

with,

$$B = \begin{bmatrix} 0 & \cos(\frac{\pi}{6}) & -\cos(\frac{\pi}{6}) \\ -1 & \sin(\frac{\pi}{6}) & \sin(\frac{\pi}{6}) \\ b & b & b \end{bmatrix}, \tag{4}$$

where b is the distance between the robot center of mass and the wheels, r is the radius of wheels, and l is the gear speed reducer.

2.2. Dynamic model

In this paper, a friction model is used to represent the balance of forces acting on the center of the robot's mass. This approach, introduced by Conceicao *et al.*[8] for wheeled mobile robots, considers the friction forces related to the orthogonal components $v(t)$ and $v_n(t)$ of the linear velocity, and the component $w(t)$ of the angular velocity of the robot's center of mass. The friction model used by Conceicao *et al.*[8] was the Coulomb + viscous friction. The Coulomb friction is proportional to the load. Therefore, the friction between the robot and the ground surface is modeled as Coulomb friction. Additionally, the viscous friction force caused by the viscosity of lubricants is assumed to have a linear relationship with the velocity.[13] This work proposes to upgrade on such modeling by including the presence of the Stiction plus the Stribeck effect. The Stiction is the friction force that acts while the system is at rest, and the Stribeck effect is the continuous passage from Stiction to friction during motion.[14] Both friction models are plotted against velocity in Fig. 4.

From the coordinates defined in Fig. 3 and Newton's second law, the equations relating translational and rotational forces acting in the robot's center of mass can be formulated as Eqs. (5), (6), and (7).

$$F_v(t) - \overbrace{B_v v(t) - \left[C_v + (F_{s_v} - C_v)\left(e^{-\left|\frac{v(t)}{vs_v}\right|^{\delta_s}}\right)\right] sgn(v(t))}^{F_{fv}} = M\frac{dv(t)}{dt}, \tag{5}$$

https://doi.org/10.1017/S0263574715000065 Published online by Cambridge University Press

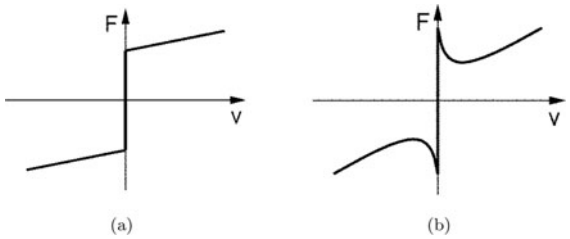


Fig. 4. Static friction models - the friction depends only on the current velocity value. (a) Coulomb + Viscous. (b) Coulomb + Viscous + Stiction + Stribeck.

$$F_{v_n}(t) - \overbrace{B_{v_n} v_n(t) - \left[C_{v_n} + (F_{s_{v_n}} - C_{v_n})\left(e^{-\left|\frac{v_n(t)}{v_{s_{v_n}}}\right|^{\delta_s}}\right)\right] sgn(v_n(t))}^{F_{fvn}} = M\frac{dv_n(t)}{dt}, \tag{6}$$

$$\Gamma(t) - \overbrace{B_w w(t) - \left[C_w + (F_{s_w} - C_w)\left(e^{-\left|\frac{w(t)}{v_{s_w}}\right|^{\delta_s}}\right)\right] sgn(w(t))}^{\Gamma_f} = J\frac{dw(t)}{dt}, \tag{7}$$

$$sgn(\alpha) = \begin{cases} 1, & \alpha > 0, \\ 0, & \alpha = 0, \\ -1, & \alpha < 0. \end{cases}$$

The viscous forces and torque are represented by $B_v v(t)$, $B_{v_n} v_n(t)$, and $B_w w(t)$, the Coulomb forces and torque by $C_v sgn(v(t))$, $C_{v_n} sgn(v_n(t))$, and $C_w sgn(w(t))$, and the Stiction forces and torque by F_{s_v}, $F_{s_{v_n}}$, and F_{s_w}. The Stribeck velocities are represented by v_{s_v}, $v_{s_{v_n}}$, and v_{s_w}, and δ_s is an adjustment parameter.[14]

F_v and F_{v_n} represent the force vectors in the robot coordinate system, and Γ represents the angular momentum about the robot's center of mass (point P). F_{fv}, F_{fvn}, and Γ_f represent the static friction models. M is the mass of the robot, and J is the moment of inertia. The relationships between the robot traction forces and the wheels' traction forces are given by

$$F_v(t) = \cos(\pi/6)(f_2(t) - f_3(t)), \tag{8}$$

$$F_{v_n}(t) = -f_1(t) + \sin(\pi/6) f_2(t) + \sin(\pi/6) f_3(t), \tag{9}$$

$$\Gamma(t) = (f_1(t) + f_2(t) + f_3(t))b. \tag{10}$$

The traction force on each wheel i (with $i = 1, 2, 3$) is given by

$$f_i(t) = \frac{T_i(t)}{r}, \tag{11}$$

where T_i is the wheel's torque. The DC motor dynamics for $i = 1, 2, 3$ can be described by the following equations:

$$u_i(t) = L_{a_i}\frac{di_{a_i}(t)}{dt} + R_{a_i} i_{a_i}(t) + K_{v_i} w_{m_i}(t), \tag{12}$$

$$T_i(t) = l K_{t_i} i_{a_i}(t), \tag{13}$$

where the u_i are the armature voltages; K_{v_i} are the emf constants; K_{t_i} are the torque constants; L_{a_i} are the armature inductances; R_{a_i} are the resistances, and i_{a_i} are the armature currents. The proposed model has the voltages of the motors as inputs and the linear and angular velocities of the robot as outputs.

https://doi.org/10.1017/S0263574715000065 Published online by Cambridge University Press

3. Parameter Estimation

This paper proposes a method based on the linear least-squares technique to combine known basis functions to estimate the viscous and Coulomb friction coefficients, and the Stiction force. The data set required for the method is obtained from sensory information about the force and velocity of the robot's center of mass, as described in Section 2. The fitting function is defined by a combination of known basis functions $\varphi_j(x)$, such that:

$$\varphi(x) = \sum_{j=1}^{m} a_j \varphi_j(x). \tag{14}$$

The coefficients a_j, for $i = j, 2, \ldots, m$, are determined by the least-squares method, such that the quadratic sum of the residues $Q(\alpha, \varphi)$, given by

$$Q(\alpha, \varphi) = \sum_{i=1}^{k} (\alpha_i - \varphi(x_i))^2 = \sum_{i=1}^{k} \left(\alpha_i - \sum_{j=1}^{m} a_j \varphi_j(x_i) \right)^2, \tag{15}$$

can be minimized. The a_j that minimizes $Q(\alpha, \varphi)$ are calculated by solving the system of linear equations

$$\begin{cases} \frac{\partial Q}{\partial a_1} = 0 \\ \frac{\partial Q}{\partial a_2} = 0 \\ \quad \vdots \\ \frac{\partial Q}{\partial a_m} = 0, \end{cases} \tag{16}$$

which is equivalent to the system of normal equations:

$$\Phi^T \Phi \mathbf{a} = \Phi^T \alpha, \tag{17}$$

where,

$$\Phi = \begin{pmatrix} \varphi_1(x_1) & \varphi_2(x_1) & \ldots & \varphi_m(x_1) \\ \varphi_1(x_2) & \varphi_2(x_2) & \ldots & \varphi_m(x_2) \\ \vdots & \vdots & \ddots & \vdots \\ \varphi_1(x_k) & \varphi_2(x_k) & \ldots & \varphi_m(x_k) \end{pmatrix}_{k \times m}, \tag{18}$$

$$\mathbf{a} = \begin{pmatrix} a_1 \\ a_2 \\ \vdots \\ a_m \end{pmatrix}, \quad \alpha = \begin{pmatrix} \alpha_1 \\ \alpha_2 \\ \vdots \\ \alpha_k \end{pmatrix}. \tag{19}$$

Rewriting the static friction model F_{fv} (see Eq. (5)) in the fitting function form for positive velocities becomes,

$$\varphi(x) = a_3 x + a_1 + (a_2 - a_1) e^{-|\frac{x}{v_{s_v}}|^{\delta_s}}, \tag{20}$$

where $\mathbf{a} = [a_1\ a_2\ a_3]^T$ are the coefficients to be determined and represent the parameters C_v, F_{s_v}, and B_v, respectively. The basis functions are defined by

$$\varphi_1(x) = 1 - e^{-|\frac{x}{v_{s_v}}|^{\delta_s}}, \quad \varphi_2(x) = e^{-|\frac{x}{v_{s_v}}|^{\delta_s}}, \quad \varphi_3(x) = x.$$

https://doi.org/10.1017/S0263574715000065 Published online by Cambridge University Press

Table I. Model parameters.

Symbol	Description	Carpet	Grass
B_v(N/m/s)	viscous friction relative to v	0.72	1.47
B_{v_n}(N/m/s)	viscous friction relative to v_n	0.82	1.16
B_ω(N/rad/s)	viscous friction relative to ω	0.012	0.011
C_v(N)	Coulomb friction relative to v	0.33	1.38
C_{v_n}(N)	Coulomb friction relative to v_n	0.15	1.09
C_ω(N.m)	Coulomb friction relative to ω	0.0079	0.082
F_{s_v}(N)	Stiction relative to v	0.80	3
$F_{s_{v_n}}$(N)	Stiction relative to v_n	0.65	2.5
F_{s_w}(N.m)	Stiction relative to ω	0.02	0.05
v_{s_v}(m/s)	Stribeck relative to v	1	1
$v_{s_{vn}}$(m/s)	Stribeck relative to v_n	1	1
v_{s_w}(rad/s)	Stribeck relative to ω	1	1
δ_s	adjustment parameter	1	1

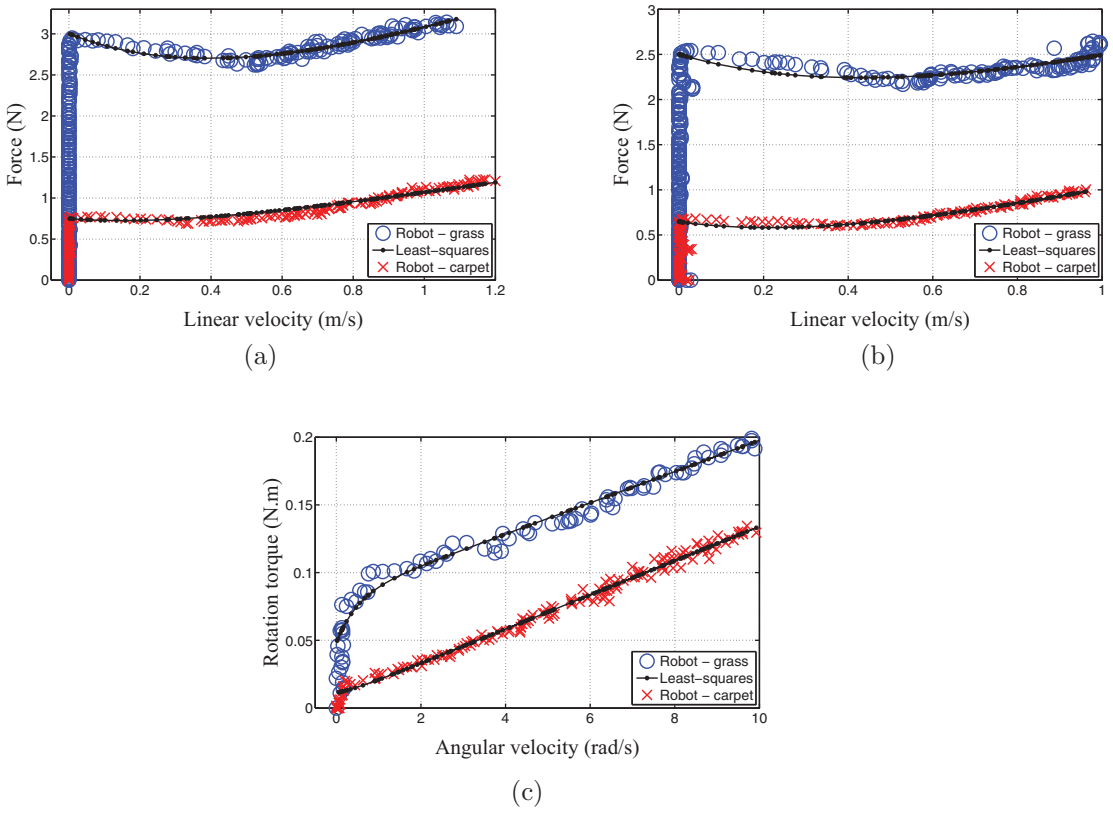


Fig. 5. Experimental data - grass and carpet. (a) F_v vs. v. (b) F_{vn} vs. v_n. (c) Γ vs. w.

The Φ matrix becomes

$$\Phi = \begin{pmatrix} 1 - e^{-\left|\frac{x_1}{v_{s_v}}\right|^{\delta_s}} & e^{-\left|\frac{x_1}{v_{s_v}}\right|^{\delta_s}} & x_1 \\ 1 - e^{-\left|\frac{x_2}{v_{s_v}}\right|^{\delta_s}} & e^{-\left|\frac{x_2}{v_{s_v}}\right|^{\delta_s}} & x_2 \\ \vdots & \vdots & \vdots \\ 1 - e^{-\left|\frac{x_k}{v_{s_v}}\right|^{\delta_s}} & e^{-\left|\frac{x_k}{v_{s_v}}\right|^{\delta_s}} & x_k \end{pmatrix}_{k \times m}, \tag{21}$$

where, for this data set, k is the number of samples, m is the number of basis functions, $x = [x_1\ x_2\ \ldots x_k]^T$ is the vector of linear velocities v, $\alpha = [\alpha_1\ \alpha_2\ \ldots \alpha_k]^T$ is the vector of traction

https://doi.org/10.1017/S0263574715000065 Published online by Cambridge University Press

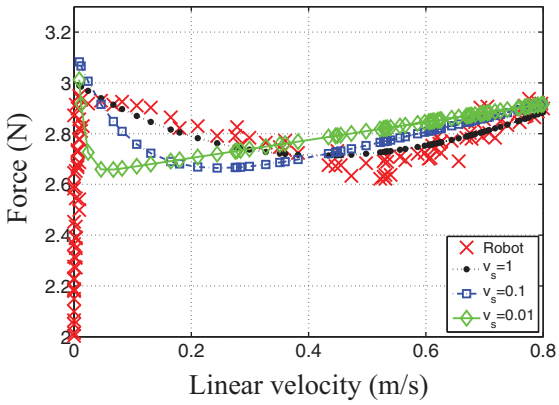


Fig. 6. F_v vs. v, plotted for different values of v_{s_v}.

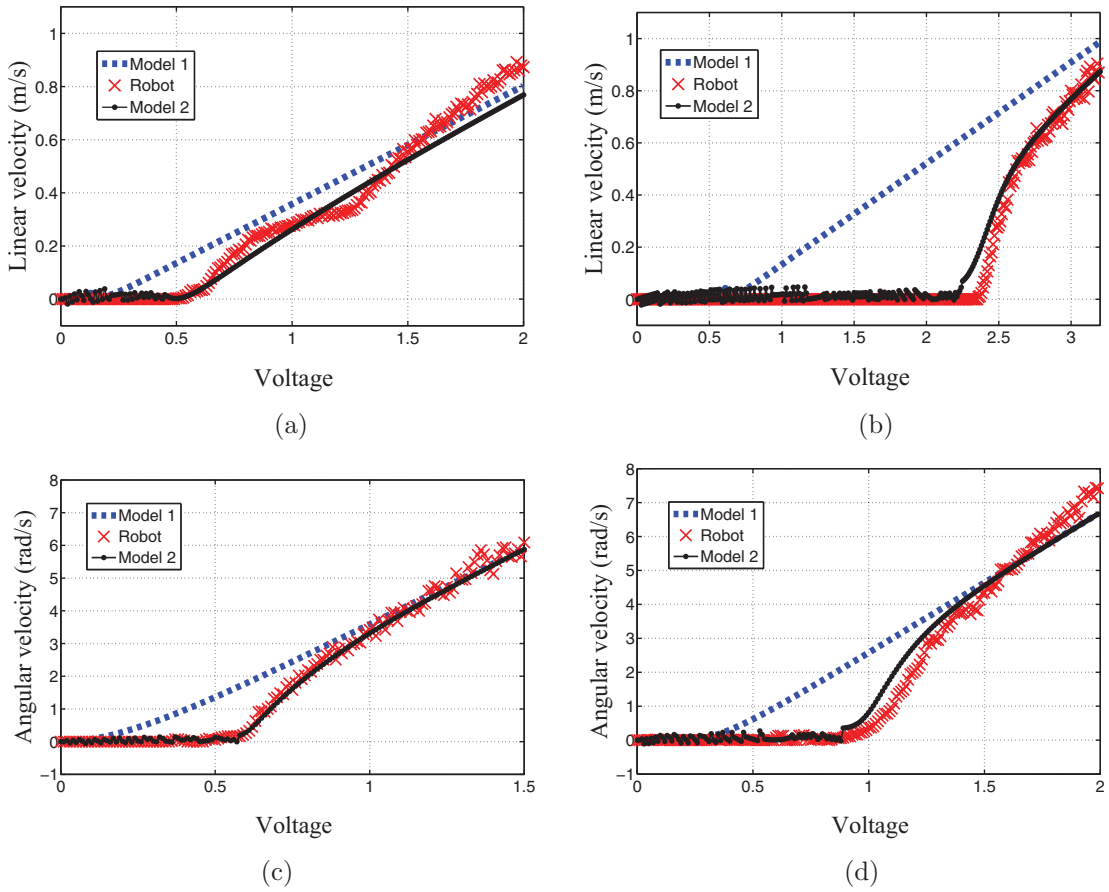


Fig. 7. Dead-zone effect. (a) Linear velocity v - carpet. (b) Linear velocity v - grass. (c) Angular velocity w - carpet. (d) Angular velocity w - grass.

forces F_v. The value of v_{s_v} is determined empirically, and the value of δ_s is commonly defined as 1.

The same analysis can be applied to Eqs. (6) and (7). The estimated parameters are presented in Table I.

4. Experimental Results and Discussion

In this section, the simulation results are compared with real navigation data on two types of floors: carpet and synthetic grass.

https://doi.org/10.1017/S0263574715000065 Published online by Cambridge University Press

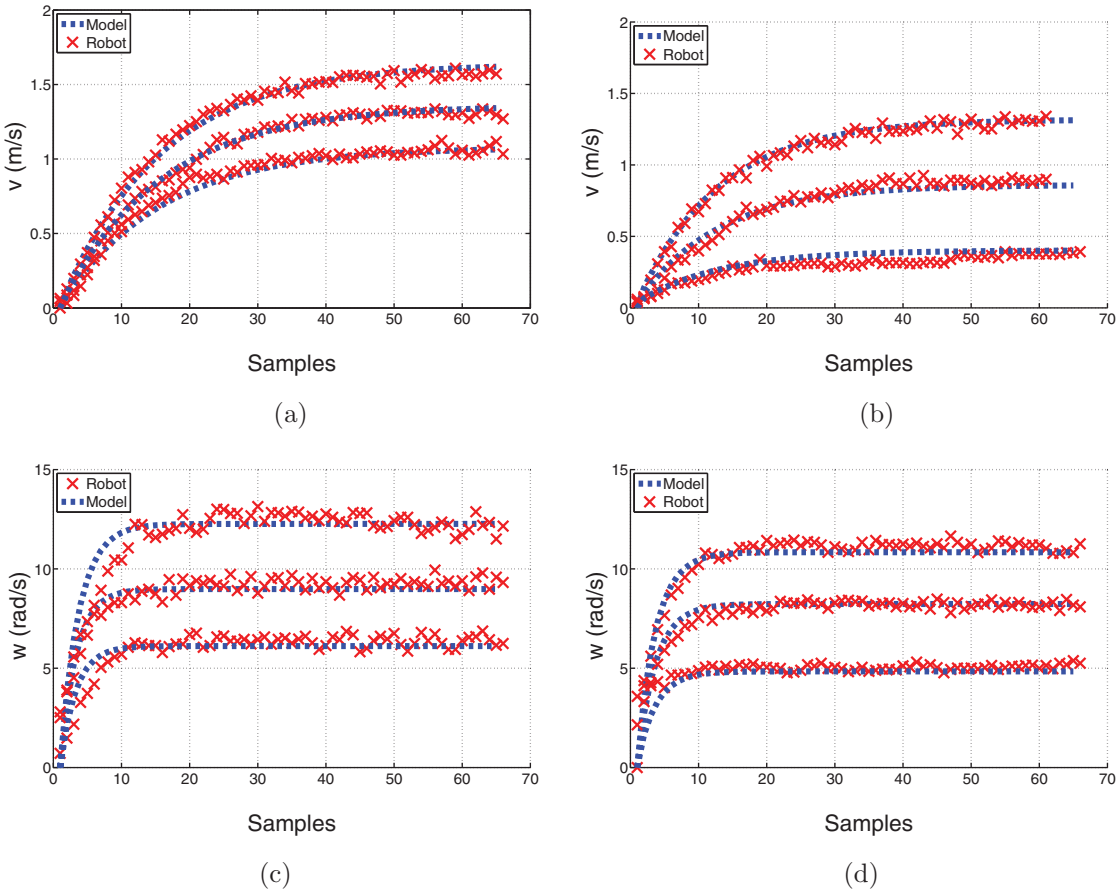


Fig. 8. Voltage step response. (a) and (b) Inputs $u(volts)$: (0; 2.5;−2.5), (0; 3; −3), (0; 3.5; −3.5). (c) and (d) Inputs $u(volts)$: (1.5; 1.5; 1.5), (2; 2; 2), (2.5; 2.5; 2.5).

Figure 5 compares the model on both carpet and synthetic grass floor. Figures 5(a) and (b) show the relationship between forces and linear velocities. Figure 5(c) shows the relationship between torque and angular velocities. As shown in Figs. 5(a) and (b), at linear velocities, the friction force decreases continuously from the static friction force level (Stribeck effect). On the other hand, the Stribeck effect can almost be neglected for angular velocities.

The Stribeck effect is the fall in the force at low velocities and the friction-velocity relation is application dependent, as analyzed in refs. [13] and [14]. Therefore, the Stribeck velocity parameter (v_{s_v}) is considered as an adjustment parameter in this work. Moreover, analyzing Eq. (20), the v_{s_v} is within the exponential parameter, and it is not possible to use the method based on the linear least-squares technique to combine known basis functions in case of including this parameter as a variable in the estimation algorithm. The influence of the Stribeck velocity parameter on the fitting curve is shown in Fig. 6. This figure shows that the value of 1 gives the best fit curve for this application (wheeled robots) in different types of floor.

A comparison between the previous work (here called Model 1) and the proposed model in this article (here called Model 2) is shown in Fig. 7. Model 1 (dashed curve) is based on a Coulomb + Viscous friction model (see Fig. 4). Model 2 considers the effect of static friction, and therefore, the open loop response should represent the dead zone. For linear velocities (Figs. 7(a) and (b)), Model 2 accurately represented the effects of the dead zone. The same did not occur with Model 1. For angular velocities (Figs. 7(c) and (d)), Model 2 also achieved good performance.

Figure 8 shows a voltage step response of the robot on synthetic grass and carpet. For example, the input $u(volts)$: (0; 2.5;−2.5), while applying 0 V in motor 1, 2.5 V in motor 2, and −2.5 V in motor 3, the linear velocity of the robot is in the direction of vector v, see Fig. 8(a). The model gives a good representation of the robot state in steady-state velocities for different voltage amplitudes.

https://doi.org/10.1017/S0263574715000065 Published online by Cambridge University Press

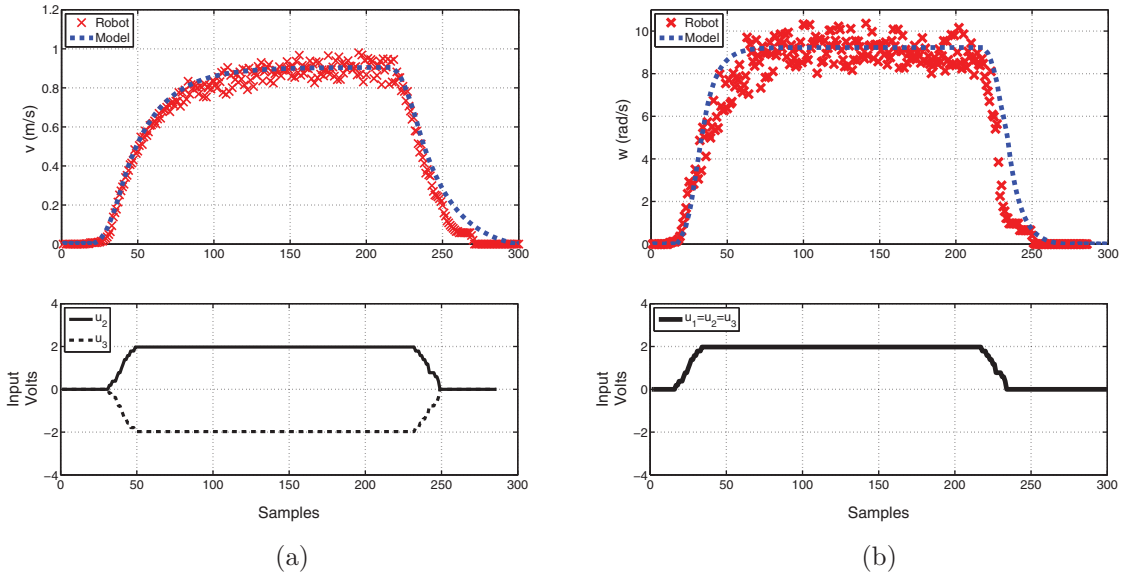


Fig. 9. Voltage step response with an initial acceleration ramp and a final deceleration ramp. (a) Linear velocity v. (b) Angular velocity w.

Figure 9 shows a voltage step response with an initial acceleration ramp and a final deceleration ramp of the robot on carpet. Again, the results show a good representation of the robot state while the robot velocity is increasing and decreasing, besides constant velocity.

5. Conclusion

A improved model for wheeled mobile robots that includes a static friction model in the force balance at the robot's center of mass and a new method for online estimation based on a least-squares technique to a linearly combine functions were proposed in this article.

The improved model considers two key friction phenomena in wheeled mobile robots (Stiction force and the Stribeck effect). The new estimation method uses the robot's speed and force to estimate the viscous and Coulomb friction coefficients, and the Stiction force. These sensory information may be from proprioceptive sensors (likely to be part of wheeled systems) or exteroceptive sensors (for example, vision-based top-view sensors).

Simulation and real robot results were presented for two types of floor (carpet and synthetic grass). The results demonstrated the adaptability of the model to different frictional forces and nonlinear effects such as dead-zones, with good accuracy and low computational cost. The proposed dynamics model was applied to a three-wheeled omnidirectional robot, but it applies to any omnidirectional robot with three or more wheels. Additionally, a comparison with a Coulomb + viscous friction model was presented. The proposed model can be useful for the design of controllers (see ref. [3]), slippage analysis, and navigation based on energy constraints. Our future work will extend this approach to models of dynamic friction and to outdoor robots.

Acknowledgments

The authors gratefully acknowledge the financial support of CAPES and CNPq.

References

1. A. Mehmood, S. Laghrouche, M. El Bagdouri and F. S. Ahmed, "Sensitivity Analysis of LuGre Friction Model for Pneumatic Actuator Control," *IEEE Vehicle Power and Propulsion Conference (VPPC)* (2010) pp. 1–6, DOI: 10.1109/VPPC.2010.5729116.
2. Z. Jia, W. Smith and H. Peng, "Fast analytical models of wheeled locomotion in deformable terrain for mobile robots," *Robotica* **31**, 35–53 (2013), DOI: 10.1017/S0263574712000069.

https://doi.org/10.1017/S0263574715000065 Published online by Cambridge University Press

3. J. C. L. Barreto S., A. G. S. Conceicao, C. E. T. Dorea, L. Martinez and E. R. de Pieri, "Design and implementation of model-predictive control with friction compensation on an omnidirectional mobile robot," *IEEE/ASME Trans. Mechatronics* **PP**(99), 1–10 (2013), DOI: 10.1109/TMECH.2013.2243161.
4. T. P. Nascimento, A. G. S. Conceição and A. P. Moreira. "Multi-robot nonlinear model predictive formation control: The obstacle avoidance problem," *Robotica* (2014) pp. 1–19, DOI: 10.1017/S0263574714001696.
5. T. H. Lee, K. K. Tan and S. Huang, "Adaptive friction compensation with a dynamical friction model," *IEEE/ASME Trans. Mechatronics* **16**(1), 133–140 (2011), DOI: 10.1109/TMECH.2009.2036994.
6. K. Shojaei, "Saturated output feedback control of uncertain nonholonomic wheeled mobile robots," *Robotica* **33**(1), 87–105 (2015), DOI: 10.1017/S0263574714000046.
7. K. Kashiwazaki, N. Yonezawa, M. Endo, K. Kosuge, Y. Sugahara, Y. Hirata, T. Kanbayashi, K. Suzuki, K. Murakami and K. Nakamura, "A Car Transportation System using Multiple Mobile Robots: iCART II," *IEEE/RSJ International Conference on Intelligent Robots and Systems (IROS)* (2011) pp. 4593–4600, DOI: 10.1109/IROS.2011.6094889.
8. A. G. S. Conceicao, A. Moreira and P. Costa, "Practical approach of modeling and parameters estimation for omnidirectional mobile robots," *IEEE/ASME Trans. Mechatronics*, **14**, 377–381 (2009), DOI: 10.1109/TMECH.2009.2013615.
9. Y. Chen, Q. Liu and T. Ren, "A simple and novel helical drive in-pipe robot," *Robotica* (2014) pp. 1–13, DOI: 10.1017/S0263574714000599.
10. G. Bayar, A. B. Koku and E. I. Konukseven, "Dynamic modeling and parameter estimation for traction, rolling, and lateral wheel forces to enhance mobile robot trajectory tracking," *Robotica* (2014) pp. 1–17, DOI: 10.1017/S0263574714001386.
11. Maxon Motor. Available on http://www.maxonmotor.com/.
12. H. P. Oliveira, A. J. Sousa, A. P. Moreira and P. J. Costa, "Modeling and Assessing of Omni-directional Robots with Three and Four Wheels," *Contemporary Robotics - Challenges and Solutions* (2009) pp. 207–229.
13. H. Olsson, K. J. Astrom, C. Canudas de Wit, M. Gafvert and P. Lischinsky, "Friction models and friction compensation," *Eur. J. Control* **4**, 176–195 (1998).
14. B. Bona and M. Indri, "Friction Compensation in Robotics: An Overview," *Proceedings of the 44th IEEE Conference on Decision and Control and European Control Conference (CDC-ECC'05)* (2005) pp. 4360–4367, DOI: 10.1109/CDC.2005.1582848.

https://doi.org/10.1017/S0263574715000065 Published online by Cambridge University Press